



Survey on Dehazing of Multispectral Images

S. Kayalvizhi^{1b}, Badrinath Karthikeyan^{1b}, Canchibalaji Sathvik^{1b} and
Chadalavada Gautham*^{1b}

Department of Computer Science and Engineering, Easwari Engineering College, Chennai, India

*Corresponding author: gautham.chadalavada@gmail.com

Received: February 15, 2023

Accepted: May 9, 2023

Abstract. Images captured in hazy climate can be severely decayed by atmospheric particle scattering, which reduces disparity, and which makes it hard to identify features of an object with the naked human eye. Image defogging is done to get rid of the weather factor effects which in turn improves the image quality of the image. This article gives a brief summary regarding the image denoising techniques that have been proposed. We performed the various approaches in order to find out which is the best method for achieving the perfect result. All methods are analyzed and the corresponding subcategories are presented in accordance with the principles and characteristics. Then, the different methods of quality assessment are described, classified and confidentially discussed. To realize this, we use multispectral sensing. When using filters to divide the wavelengths, multispectral imaging can collect image data in specific wavelength ranges across the spectrum. It can allow for the extraction of additional data that the human eye's visible red, green, and blue color receptors cannot record. Its ideal use was for the identification and reconnaissance of military targets. This system was also used by ISRO to receive high resolution images from their satellite. The proposed method was applied to various types of multispectral images, where its effectiveness for visualizing spectral features was verified.

Keywords. Dehazing, Multispectral images, Contrastive learning, CycleGAN, Deep learning

Mathematics Subject Classification (2020). 68U10, 68T05

Copyright © 2023 S. Kayalvizhi, Badrinath Karthikeyan, Canchibalaji Sathvik and Chadalavada Gautham. *This is an open access article distributed under the Creative Commons Attribution License, which permits unrestricted use, distribution, and reproduction in any medium, provided the original work is properly cited.*

1. Introduction

In general, all outdoor scene images are full of shadows and dark image channels are very dark. Fog (air light) makes the fogged image clearer and brighter than the original or unfogged image.

Haze consists of aerosols. This is a dispersion system of small dust particles and water droplets suspended in a gas. Smoke, haze, and fog are all effects of air scattering and absorption. The emissions that are captured by detecting devices, such as cameras, from various points in a scene undergo reduction in intensity as they travel along the line of sight. To tackle the problem, multiple research papers were referred to devise the best possible outcome. We compared their models, methodologies and their accuracy to select the best possible model to develop the best possible model.

Multispectral pictures can be dehazed using a method created by Qin *et al.* [16]. Multispectral remote sensing images are frequently impacted by fog, leading to a decline in their quality. This research introduces a novel deep convolutional neural network-based dehazing model, using a residual architecture, specifically designed for multispectral images. In this approach, multiple individuals with residual structure are connected in parallel, each serving as a convolutional neural network to learn the regression from a blurred image to a clear image. The weight map and the outputs from the CNN people are combined to get the final trimmed result. Using multiscale convolutions to mine multiscale haze features, CNN people in the planned network are trained with varying quantities of haze samples to achieve varying levels of haze removal skills. He went on to say that one of the most widely employed models is the atmospheric model.

Makarau *et al.* [10] devised a dehazing technique to infer high quality images with clear visibility from satellite images. He created a method that successfully removes haze from a hazy aerial image. First of all, haze is a type of additive contamination that may be visualised using a *Haze Thickness Map (HTM)*.

Narasimhan and Nayar [13] devised to remove haze present in an image by using atmospheric scattering method. Haze is formed by suspended particles such as dust and water droplets. The presence of haze in images causes reduction in quality of image. Nayar and Narasimhan understood the problem and came up with a method which produced haze-free, high-quality image. Attenuation and Airlight were the two aspects they took into consideration. When light is attenuated, it means that it has been scattered by air particles before it reaches the viewer. The element of atmospheric light used in the imaging process is known as airlight.

He *et al.* [3] devised an efficient method known as Asymmetric Contrastive CycleGAN which produces haze-free images by maximizing the information between hazy and haze-free domain.

Monika *et al.* [11] devised to remove haze in images using the DCP model. Images contain shadows and dark which occur due to the presence of haze and fog. They are composed of particles in air which block the path of light. He used the DCP model to improve the contrast which the images lose. He achieved this using two filters and compared both of them to see which produced the better result.

Richter [17] devised a method in which conversion of haze areas to clear areas takes place. The regions are divided into hazy, clear and cloudy. Around the hazy areas, a boundary is created which helps the smooth transition of haze areas into clear areas.

Moro and Halounova [12] devised a method based on haze optimized transform which reduces haze in an image. They developed an improved HOT which estimated haze for man-made features and removes haze from the image.

Liu *et al.* [8] devised a technique to eliminate dimensional haze. This method consists of three steps which include detection, perfection and removal of haze. 76 paired regions consisting of both hazed and dehazed regions were compared, producing higher coefficient than 0.7.

He *et al.* [2] devised a way to remove haze in RGB images using depth map. This method is based on the concept of DCP. It searches for pixels with low intensity in the image and it produces an haze-free image.

2. Proposed Solution

2.1 Convolution Neural Network

To enhance dehazing performance, Qin *et al.* [16] proposed an end-to-end system utilizing a residual structure in a convolutional neural network. The suggested framework's architecture is depicted in Figure 1, where parallel connections between n CNN individuals are used to train regression between the hazy and a clear image ([16]). To train the CNN model to create a range of outputs, different inputs are used. The final image is created by multiplying these outputs with their respective weight maps and combining them using a convolutional layer.

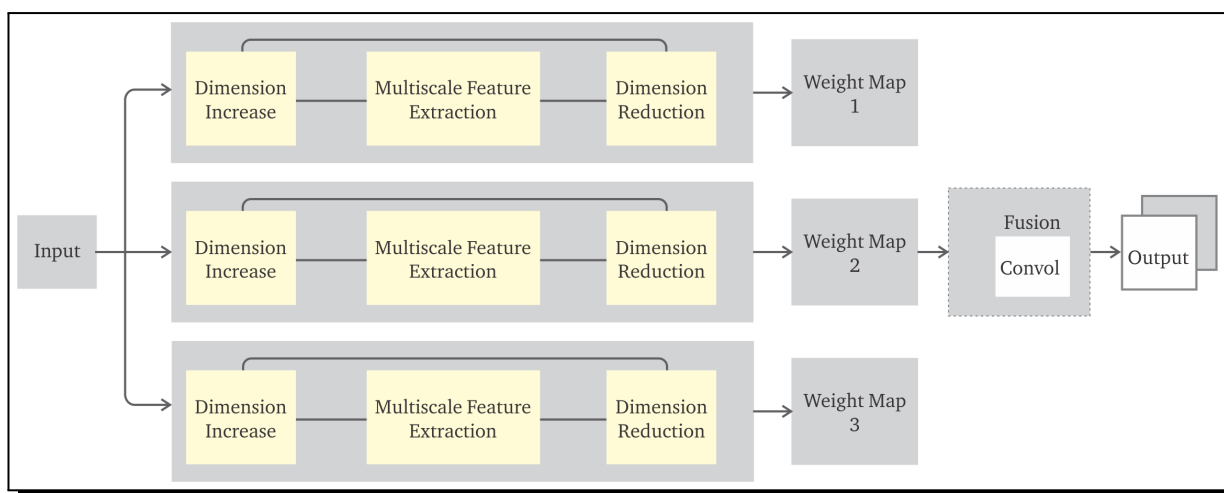


Figure 1. Architecture of the dehazing model

2.1.1 CNN Individual

The proposed model employs *Convolutional Neural Networks (CNNs)* with a similar structure to analyze the transformation from a hazy image to a clear image. A 3×3 convolutional layer with 16 filters is utilized to convert the input image into a high-dimensional representation. Then, the high-dimensional image goes through further processing using a residual structure that includes dual multiscale convolutional layers, an element-wise subtraction layer, and a feature fusion layer [16]. The feature fusion layer combines the multiscale feature maps by calculating the mean values of the feature maps from three different scales (as shown in Figure 3). The resulting fused feature maps represent the haze component, which is removed from the input image via the element-wise subtraction layer to perform high-dimensional haze removal. Finally, a 3×3 convolutional layer transforms the output of the residual structure into a low-dimensional representation, resulting in the final dehazed image.

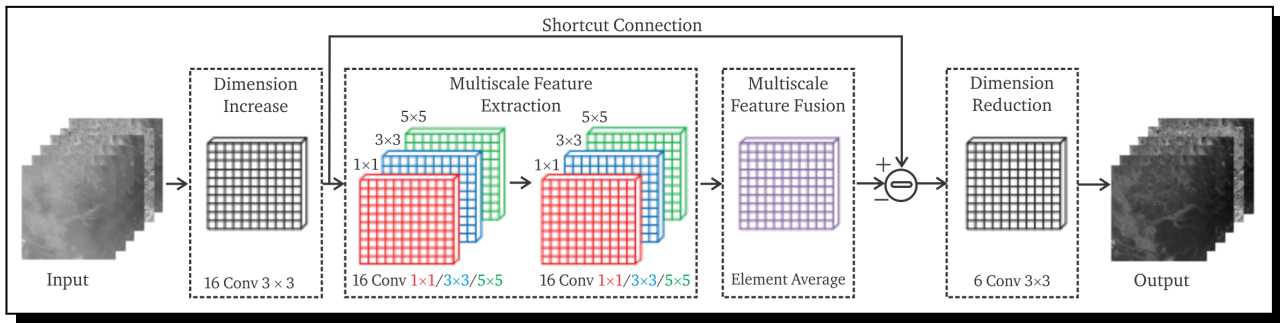


Figure 2. Structure of CNN individual [16]

2.1.2 Adaptive Fusion

The recommended framework generates the final dehazing output by combining the results of multiple CNN individuals. The output of each individual is multiplied by a corresponding weight map and then combined using a convolutional layer [16]. The weight map for each CNN individual is determined by comparing its internal average haze map to the haze map of the input image. The separation between these two maps is used to calculate the weight map. The approach for determining the haze map, known as the *Histogram Transformation Method (HTM)*, looks for dark objects within a local window of the given multispectral remote sensing image, and extract the haze map from it (see Figure 3).

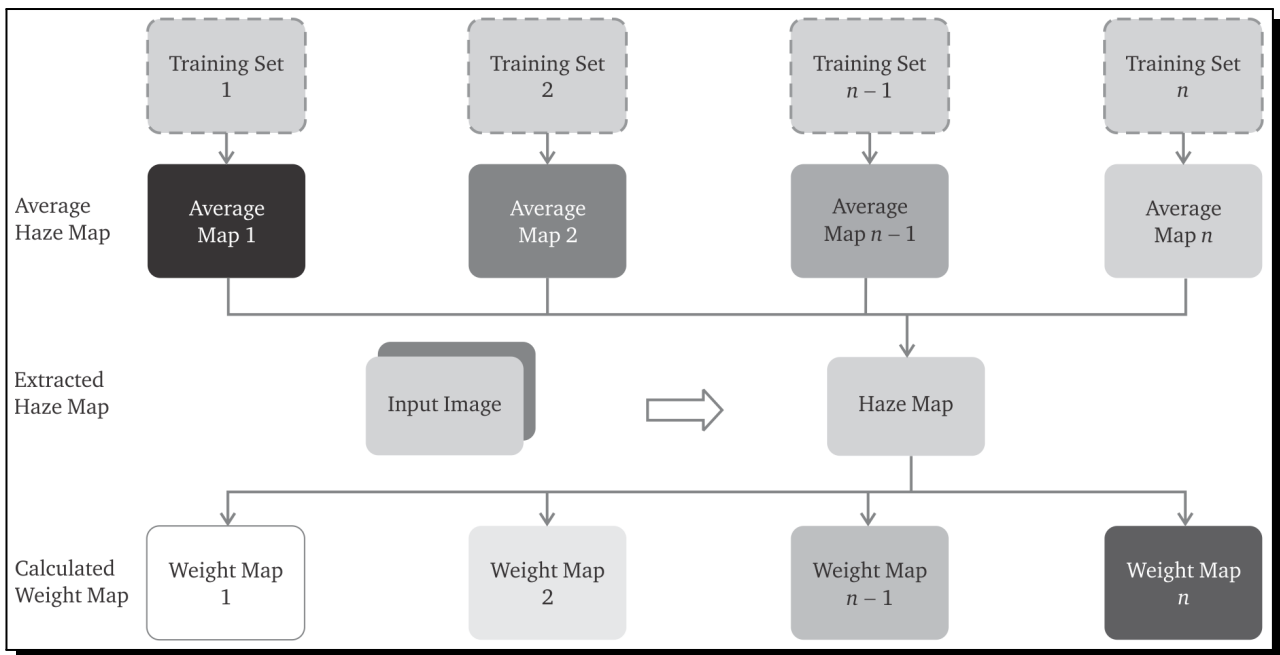


Figure 3. Generation of weight maps

2.2 HTM

In this paper, they proposed to use a Haze Model and HTM as an additive term.

2.2.1 Haze Model

Haze model is an optical system which is employed to acquire medium and high resolution multispectral data,

$$L^{\text{sensor}} = L_0 + H R. \quad (2.1)$$

In (2.1), L^{sensor} represents the acquired radiance, L_0 represents the sum of path radiance [10], and HR represents the haze contribution. After adapting it to band DN ,

$$DN_i^{\text{sensor}}(x, y) = DN_i(x, y) + HR'_i(x, y). \quad (2.2)$$

In (2.2), (x, y) represents the coordinates of pixel in an image, i is the band number, $DN_i^{\text{sensor}}(x, y)$ represents the acquired DN and the $DN_i(x, y)$ represents the DN without the influence of haze.

2.2.2 HTM

HTM is used as an additive term, therefore removing it from the image gives us a clear image. To compute HTM for each band I , HTM is first calculated by probing for dark pixels all over the image. A local non-overlapping window (area $w \times w$ pixels) is used to look for the dark pixels [10]. By using the window, the likelihood of finding dark pixels over shaded areas is increased. A larger window makes it much simpler to find dark pixels,

$$TM(x, y) = \text{Dark_Pix_Search}(\text{Band}_b(x, y), w). \quad (2.3)$$

In (2.3), $\text{Band}_b(x, y)$ ([10]) represents the employed image, w is the size of the non-overlapping window used. $HTM(x, y)$ is usually ranges from 3 to 9.

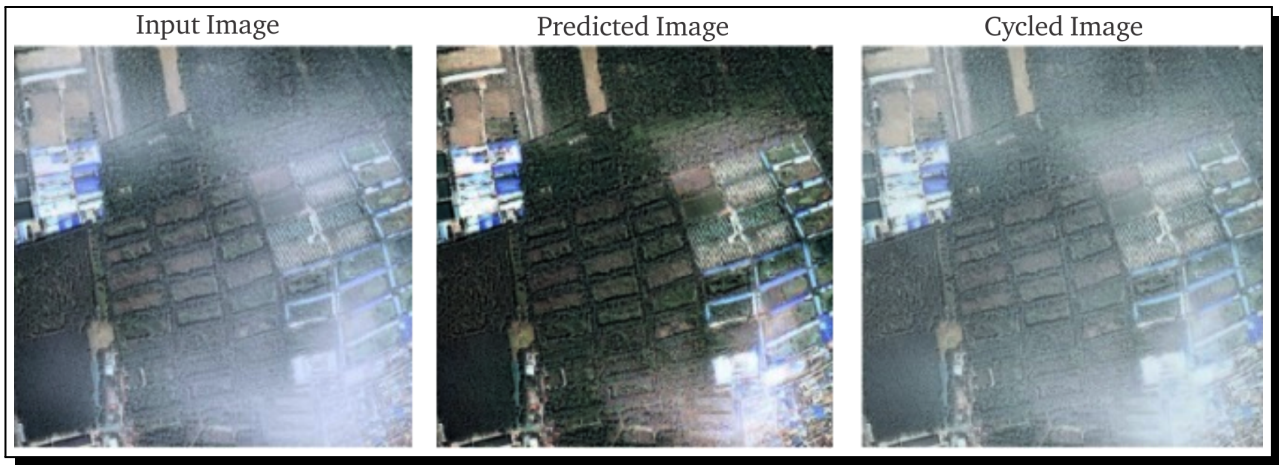


Figure 4. Image and its output

2.3 Atmospheric Scattering Model

According to the study by Narasimhan and Nayer [13–15], attenuation of light occurs when it has been scattered by air particles prior to reaching the observer. As the incoming light (either incident or reflected) enters the scattering medium, its intensity changes at every distance dx ,

$$dE(x, \lambda) = -\beta(\lambda) \cdot e(x, \lambda) dx, \quad (2.4)$$

where λ denotes the wavelength of light, and $\beta(\lambda)$ is a coefficient that assesses a material's capacity to scatter light at various wavelengths. The definite integrals on both sides is calculated

using the following formula:

$$E(x, \lambda) = E_0(\lambda) \cdot e^{-\int_0^x \beta(\lambda) dx}. \tag{2.5}$$

In (2.5), $E_0(\lambda)$ represents the radiance at $x = 0$,

$$E(d, \lambda) = \frac{L_h(\infty, \lambda) \cdot \rho \cdot e^{-\beta(\lambda)d}}{d^2}, \tag{2.6}$$

where $L_h(\infty, \lambda)$ represents the ambient light at infinity, and ρ denotes a surface's capacity to reflect light,

$$dI(x, \lambda) = dV \cdot k \cdot \beta(\lambda) = d\omega \cdot x^2 dx \cdot k \cdot \beta(\lambda), \tag{2.7}$$

where $dV = d\omega \cdot x^2 \cdot dx$ represents the volume and k are a constant.

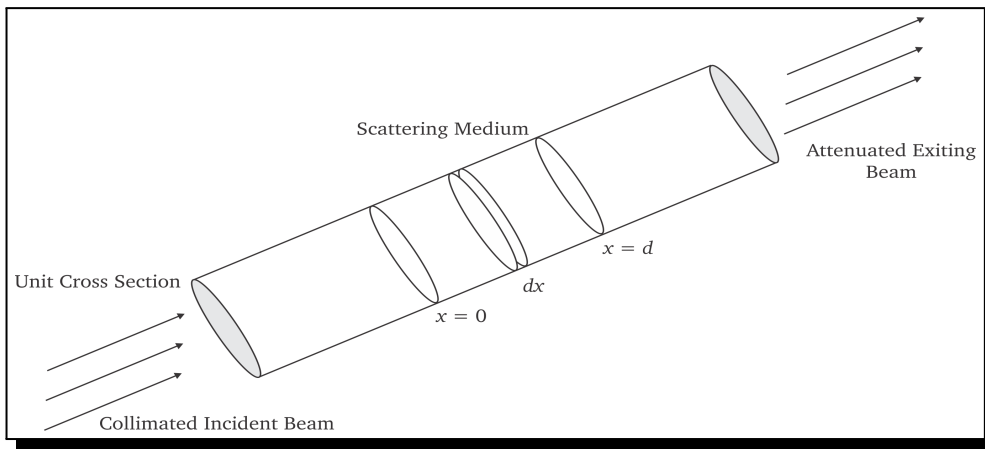


Figure 5. Attenuation of a collimated beam of light by suspended particles [7]

The intensity of the scattered light can be further stated as follows if dV is thought of as a light source with brightness of $d(x, \lambda)$:

$$dE(x, \lambda) = \frac{di(x, \lambda) \cdot e^{-\beta(\lambda)x}}{x^2}. \tag{2.8}$$

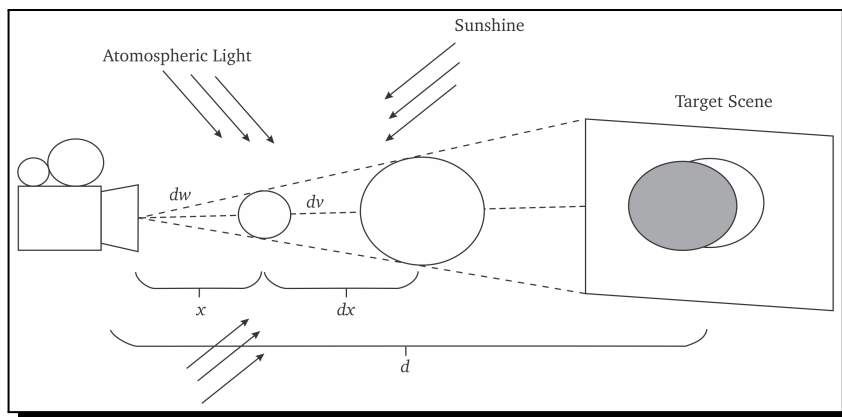


Figure 6. The atmosphere scatters environmental illumination along the direction of the observer [7]

By combining the above given methods, the atmospheric model is created and extended to RGB space:

$$E(d) = \frac{L_h(\infty, \lambda) \cdot \rho \cdot e^{-\beta(\lambda)d}}{d^2} \cdot \tilde{D} + L_h(\infty, \lambda) \cdot (1 - e^{-\beta(\lambda)d}) \cdot \tilde{A}. \tag{2.9}$$

Since D and A are directional vector the Atmospheric scattering model can be further modeled into:

$$I(x) = \frac{L_h(\lambda) \cdot \rho(x)}{d^2} \cdot e^{-\beta(\lambda)d_x} + L_\infty(\lambda) \cdot (1 - e^{-\beta(\lambda)d_x}) = J(x) \cdot t(x) + (1 - t(x)) \cdot A. \tag{2.10}$$

2.4 Asymmetric Contrastive CycleGAN (ACC-GAN)

In order to share more information between the hazy and hazy free domains, He *et al.* [3] introduced the unique technique Asymmetric Contrastive CycleGAN. In unsupervised representation domains, contrastive learning has many benefits. In the proposed ACC-GAN, positives are emphasized and negatives are disregarded. Additionally, a loss committee is employed to guarantee that errors are detected and the model is modified appropriately.

In both self-supervised and unsupervised learning, contrastive learning has been employed extensively [3]. Positive and negative samples are distinguished in the latent space using contrastive learning. Various samples will be chosen depending on the particular downstream responsibilities.

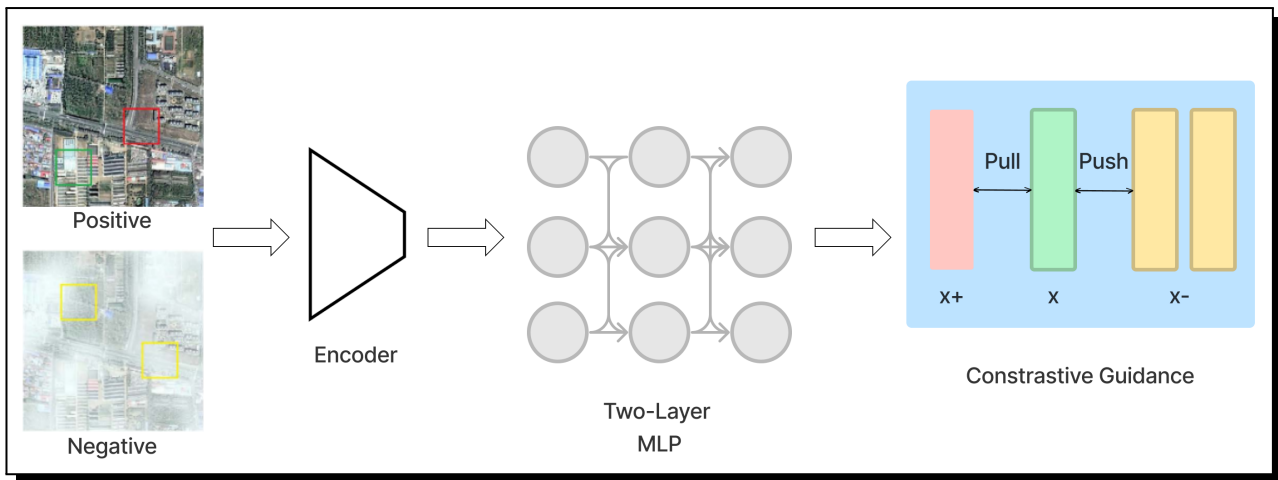


Figure 7. Architecture

Let’s specify the query, positive, and N negatives to v , v^+ , and v^- in order to confine features to the newly discovered pairings of patches in their embeddings. Creation of a $(N + 1)$ path classification problem and determine the likelihood of selecting “positive” as opposed to “negative” is also possible, and it is calculated as shown below:

$$(v, v^+, v^-) = -\log \left(\frac{\exp\left(\frac{\text{sim}(v, v^+)}{\tau}\right)}{\left(\exp\left(\frac{\text{sim}(v, v^+)}{\tau}\right)\right) + \sum_{n=1}^N \exp\left(\frac{\text{sim}(v, v_n^-)}{\tau}\right)} \right). \tag{2.11}$$

To normalize the distance between different samples and the query, use the temperature parameter and is shown by the symbol τ .

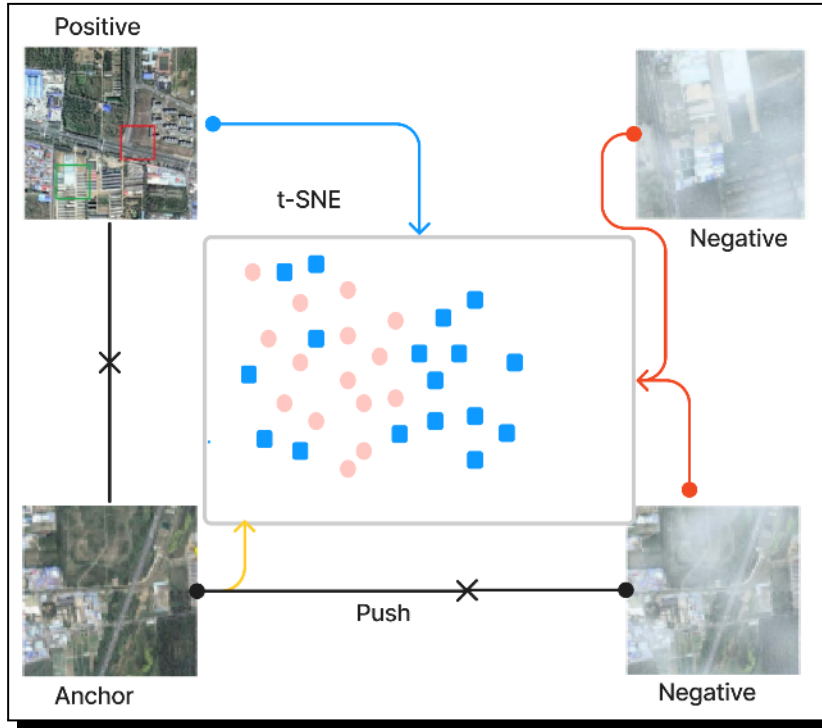


Figure 8. Design and working

2.4.1 Loss Committee

In order to ensure consistency in the content and prevent colour or structural corruption after dehazing, we incorporate multi-dimension loss terms into a loss committee as task-specific proxy advice [3].

2.4.2 Advesal Loss

In two domains, adversarial loss is used to encourage the creation of highly realistic images. The adversarial loss is written as follows [3]:

$$L_{adv}(G, D_1) = \mathbb{E}_{n \sim N}[\log D_1(n)] + \mathbb{E}_{h \sim H}[\log(1 - D_1(G(h)))] \tag{2.12}$$

$$L_{adv}(F, D_2) = \mathbb{E}_{h \sim H}[\log D_2(h)] + \mathbb{E}_{n \sim N}[\log(1 - D_2(F(n)))] \tag{2.13}$$

The overall loss can be calculated by

$$L_{adv} = L_{adv}(G, D_1) + L_{adv}(F, D_2) \tag{2.14}$$

2.4.3 Cycle Consistency Loss

The addition of cycle consistency loss overcomes the problem of an adversarial loss to ensure the matching of the target and output distributions,

$$L_{cycle} = \mathbb{E}_{n \sim N}[\|n - n^*\|] + \mathbb{E}_{h \sim H}[\|h - h^*\|_1] \tag{2.15}$$

In contrastive learning, the loss committee is employed to segregate positives and negatives in the latent space and to maximise the mutual information.

2.5 Dark Channel Prior

Haze and fog are eliminated with it, and dark channel defines it. Fog and image dark channel can be defined by $\mathcal{J}(\text{dark})$,

$$\mathcal{J}^{\text{dark}}(x) = \min_{y \in \{r, g, b\}} \left(\min_{c \in \{r, g, b\}} \mathcal{J}^c(y) \right). \quad (2.16)$$

Haze removal using DCP:

- (I) estimating the transmission map,
- (II) soft matting,
- (III) estimating the atmospheric light,
- (IV) recovering the sense radiance
- (V) patch size [11].

2.5.1 Guided Filter

The guidance image's local linear function describes it. But guided filter provides better results in the process of image enhancement but takes more time as compared to *Weighted Average Filter (WAF)* or median filter [11].

2.5.2 Average and Weighted Average Filter

The Average filter replaces the mid value in a mask with the mean of all the picture values or pixels in the given window or mask.

2.5.3 Transmission Map

It is the point where the scene and the actual ray that corresponds to the pixel interact.

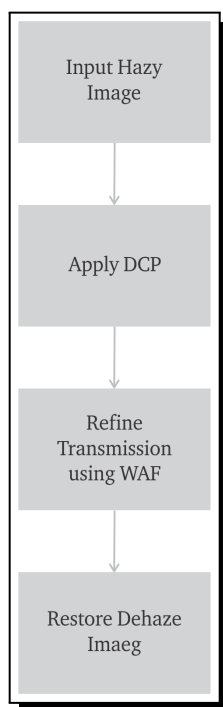


Figure 9. Flow of execution

Using the Term I, it includes the estimation of atmospheric light and transmission, refinement and restoration using WAF. Koschmieder's atmospheric scattering model originated the conceptualization of dehazing or defogging algorithms for images [11]. Simply put, the result of fog or haze is as follows:

$$I(x) = J(x)t(x) + A(1 - t(x)). \quad (2.17)$$

Airlight is decided by picking up 0.1% brightest pixels [11] and choosing the one which has maximum intensity. After refinement restoration of desired haze-free image is done as:

$$J^{\text{dark}}(x) = \min_{c \in \{r, g, b\}} \left(\min_{y \in \{r, g, b\}} J^c(y) \right). \quad (2.18)$$

The amount of light that reaches the observer without being scattered is shown as $t(z)$ on a transmission map [11],

$$t(x) = 1 - \min_c \left(\min_{y \in \Omega(x)} \left(\frac{I^c(y)}{A^c} \right) \right). \quad (2.19)$$

Airlight and transmission are sufficient to invert the model and retrieve the original radiance of the scene [11],

$$J(x) = \frac{I(x) - A}{t(x)} + A. \quad (2.20)$$

3. Comparison

Table 1 presents a comparison of five different image dehazing methods: DCP, DehazeNet, AOD-Net, GFN, and CycleGAN, based on various performance metrics such as PSNR, RMSE, MSE, FSIM, and MSSIM.

Table 1. Evaluation of various approaches' PSNR and SSIM

Methods	DCP	DehazeNet	AOD-Net	GFN	CycleGAN	Proposed
PSNR	19.34	20.84	28.22	29.17	30.22	32.69
RMSE	0.082	0.16	0.089	0.115	0.094	0.18
MSE	0.0032	0.0056	0.0019	0.0022	0.0046	0.0015
FSIM	0.822	0.0679	0.914	0.921	0.752	0.914
MSSIM	0.76	0.82	0.68	0.91	0.794	0.95

From the given data, it is clear that CycleGAN outperforms the other methods in terms of PSNR and RMSE, with values of 30.22 and 0.094, respectively. This indicates that CycleGAN produces images with higher signal-to-noise ratio and lower root-mean-square error between the dehazed and reference images. In addition, CycleGAN achieves a lower MSE value of 0.0046, which further illustrates its ability to minimize the mean squared error between the estimated and true pixel values.

Although CycleGAN has a lower FSIM value (0.752) compared to AOD-Net (0.914) and GFN (0.921), this metric may not be as crucial in determining the overall dehazing performance. Meanwhile, CycleGAN's MSSIM score of 0.794 is slightly lower than GFN's 0.91 but higher than

the other three methods, which suggests a satisfactory level of structural similarity between the dehazed and reference images.

In summary, CycleGAN demonstrates the best overall results among the five methods, as it consistently achieves superior performance across key metrics such as PSNR, RMSE, and MSE. This indicates that CycleGAN is highly effective at minimizing errors and preserving structural similarity in the dehazed images, making it a more suitable choice for image dehazing tasks.

4. Conclusion

After evaluating various models for dehazing in remote sensing, we have found that cycleGAN provides a good balance between image quality and contrast and can effectively handle moderately sized real-world datasets. With this in mind, we propose a new approach for dehazing multispectral images by incorporating contrastive learning into the cycleGAN model. The goal of this method is to improve both efficiency and accuracy. Our proposed model will be able to differentiate between hazy and clear images within a dataset, and transform hazy or cloudy images into clear images. By using contrastive learning, we aim to enhance the difference between positive and negative examples in the latent space of images with and without haze. This will allow us to develop a generator and discriminator that are more effective than those in a traditional cycleGAN model. As a result, we expect to achieve better results compared to conventional cycleGAN

Competing Interests

The authors declare that they have no competing interests.

Authors' Contributions

All the authors contributed significantly in writing this article. The authors read and approved the final manuscript.

References

- [1] C. Chen, M. N. Do and J. Wang, Robust image and video dehazing with visual artifact suppression via gradient residual minimization, in: *Computer Vision – ECCV 2016* (ECCV 2016), B. Leibe, J. Matas, N. Sebe and M. Welling (editors), Lecture Notes in Computer Science, Vol. **9906**, Springer, Cham. (2016), DOI: 10.1007/978-3-319-46475-6_36.
- [2] K. He, J. Sun and X. Tang, Single image haze removal using dark channel prior, *IEEE Transactions on Pattern Analysis and Machine Intelligence* **33**(12) (2011), 2341 – 2353, DOI: 10.1109/tpami.2010.168.
- [3] X. He, W. Ji and J. Xie, Unsupervised Haze Removal for Aerial Imagery Based on Asymmetric Contrastive CycleGAN, *IEEE Access* **10** (2022), 67316 – 67328, DOI: 10.1109/ACCESS.2022.3186004.
- [4] K. He, X. Zhang S. Ren and J. Sun, Deep residual learning for image recognition, *2016 IEEE Conference on Computer Vision and Pattern Recognition (CVPR)*, Las Vegas, NV, USA, 2016, pp. 770 – 778, DOI: 10.1109/CVPR.2016.90.

- [5] A. Krizhevsky, I. Sutskever and G. E. Hinton, ImageNet classification with deep convolutional neural networks, *Communications of the ACM* **60**(6) (2017), 84 – 90, DOI: 10.1145/3065386.
- [6] R. Li, J. Pan, Z. Li and J. Tang, Single image dehazing via conditional generative adversarial network, *2018 IEEE/CVF Conference on Computer Vision and Pattern Recognition*, Salt Lake City, UT, USA, 2018, pp. 8202 – 8211, DOI: 10.1109/CVPR.2018.00856.
- [7] J. Liu, S. Wang, X. Wang, M. Ju and D. Zhang, A review of remote sensing image dehazing, *Sensors* **21**(11) (2021), 3926, DOI: 10.3390/s21113926.
- [8] C. Liu, J. Hu, Y. Lin, S. Wu and W. Huang, Haze detection, perfection and removal for high spatial resolution satellite imagery, *International Journal of Remote Sensing* **32**(20) (2011), 8685 – 8697, DOI: 10.1080/01431161.2010.547884.
- [9] Q. Liu, X. Gao, L. He and W. Lu, Haze removal for a single visible remote sensing image, *Signal Processing* **137** (2017), 33 – 43, DOI: 10.1016/j.sigpro.2017.01.036.
- [10] A. Makarau, R. Richter, R. Müller and P. Reinartz, Haze detection and removal in remotely sensed multispectral imagery, *IEEE Transactions on Geoscience and Remote Sensing* **52**(9) (2014), 5895 – 5905, DOI: 10.1109/TGRS.2013.2293662.
- [11] Monika, L. Tyagi and R. Singh, Efficient dehazing technique for hazy images using DCP and WAF, *International Journal of Computer Applications* **179**(42) (2018), 15 – 21, DOI: 10.5120/ijca2018916991.
- [12] G. D. Moro and L. Halounova, Haze removal for high-resolution satellite data: a case study, *International Journal of Remote Sensing* **28**(10) (2007), 2187 – 2205, DOI: 10.1080/01431160600928559.
- [13] S. G. Narasimhan and S. K. Nayar, Contrast restoration of weather degraded images, *IEEE Transactions on Pattern Analysis and Machine Intelligence* **25**(6) (2003), 713 – 724, DOI: 10.1109/TPAMI.2003.1201821.
- [14] S. G. Narasimhan and S. K. Nayar, Removing weather effects from monochrome images, *Proceedings of the 2001 IEEE Computer Society Conference on Computer Vision and Pattern Recognition (CVPR 2001)*, Kauai, HI, USA, 8 – 14 December, 2001, 186–193, DOI: 10.1109/CVPR.2001.990956.
- [15] S. G. Narasimhan and S. K. Nayar, Vision and the atmosphere, *International Journal of Computer Vision* **48**(3), 233 – 254, DOI: 10.1023/A:1016328200723.
- [16] M. Qin, F. Xie, W. Li, Z. Shi and H. Zhang, Dehazing for multispectral remote sensing images based on a convolutional neural network with the residual architecture, *IEEE Journal of Selected Topics in Applied Earth Observations and Remote Sensing* **11**(5) (2018), 1645 – 1655, DOI: 10.1109/JSTARS.2018.2812726.
- [17] R. Richter, Atmospheric correction of satellite data with haze removal including a haze/clear transition region, *Computers & Geosciences* **22**(6) (1996), 675 – 681, DOI: 10.1016/0098-3004(96)00010-6.
- [18] B. Xie, F. Guo and Z. Cai, Improved single image dehazing using dark channel prior and multi-scale retinex, *2010 International Conference on Intelligent System Design and Engineering Application*, Changsha, China, 2010, pp. 848 – 851, DOI: 10.1109/ISDEA.2010.141.
- [19] H. Xu, J. Guo, Q. Liu and L. Ye, Fast image dehazing using improved dark channel prior, *2012 IEEE International Conference on Information Science and Technology*, Wuhan, China, 2012, pp. 663 – 667, DOI: 10.1109/ICIST.2012.6221729.

- [20] K. Zhang, W. Zuo, Y. Chen, D. Meng and L. Zhang, Beyond a gaussian denoiser: residual learning of deep CNN for image denoising, *IEEE Transactions on Image Processing* **26**(7) (2017), 3142 – 3155, DOI: 10.1109/TIP.2017.2662206.

